

BAU Journal - Science and Technology

Volume 1 | Issue 2
ISSN: 2706-784X

Article 8

June 2020

Dielectric properties of $\text{Cu}_{0.5}\text{Tl}_{0.5}\text{Ba}_2\text{Ca}_2\text{Cu}_3\text{O}_{10-\delta}$ superconductor added with nano- Fe_2O_3

Aly Abou-Aly

Professor, Faculty of Science, Alexandria University, Moharam Bek, Alexandria, Egypt,
aly_abou_aly@yahoo.com

Ibrahim Ibrahim

Professor, Faculty of Science, Alexandria University, Moharam Bek, Alexandria, Egypt,
ibrahim@yahoo.com

Nayera Mohammed

Professor, Faculty of Science, Alexandria University, Moharam Bek, Alexandria, Egypt,
nysharaf@yahoo.com

Mona Rekaby

Assistant Professor, Faculty of Science, Alexandria University, Moharam Bek, Alexandria, Egypt,
mona2sci@yahoo.com

Follow this and additional works at: <https://digitalcommons.bau.edu.lb/stjournal>



Part of the [Architecture Commons](#), [Business Commons](#), [Engineering Commons](#), and the [Physical Sciences and Mathematics Commons](#)

Recommended Citation

Abou-Aly, Aly; Ibrahim, Ibrahim; Mohammed, Nayera; and Rekaby, Mona (2020) "Dielectric properties of $\text{Cu}_{0.5}\text{Tl}_{0.5}\text{Ba}_2\text{Ca}_2\text{Cu}_3\text{O}_{10-\delta}$ superconductor added with nano- Fe_2O_3 ," *BAU Journal - Science and Technology*. Vol. 1 : Iss. 2 , Article 8.

Available at: <https://digitalcommons.bau.edu.lb/stjournal/vol1/iss2/8>

This Article is brought to you for free and open access by Digital Commons @ BAU. It has been accepted for inclusion in BAU Journal - Science and Technology by an authorized editor of Digital Commons @ BAU. For more information, please contact ibtihal@bau.edu.lb.

Dielectric properties of $\text{Cu}_{0.5}\text{Tl}_{0.5}\text{Ba}_2\text{Ca}_2\text{Cu}_3\text{O}_{10-\delta}$ superconductor added with nano- Fe_2O_3

Abstract

A series of high-temperature superconducting samples of type $\text{Cu}_{0.5}\text{Tl}_{0.5}\text{Ba}_2\text{Ca}_2\text{Cu}_3\text{O}_{10-\delta}$, ($\text{Cu}_{0.5}\text{Tl}_{0.5}$)-1223, added with nano- Fe_2O_3 (0.0- 1.0 wt. %) was prepared by a solid-state reaction technique via short time preparation procedure and under ambient pressure. The prepared samples were characterized using X-ray powder diffraction (XRD), scanning electron microscopy (SEM) and energy dispersive X-ray (EDX) for phase analysis and microstructure examination. The volume fraction results indicated that nano- Fe_2O_3 addition was significant in enhancing the formation rate of the ($\text{Cu}_{0.5}\text{Tl}_{0.5}$)-1223 phase, especially for $x \leq 0.2$ wt. % samples. The electrical resistivity of the prepared samples was measured by the conventional four-probe technique from room temperature down to the zero superconducting transition temperature (T_0). An increase in the superconducting temperature, T_c , is observed up to $x = 0.2$ wt. %, followed by a systematic decrease with increasing nano- Fe_2O_3 addition. The dielectric constants (ϵ' and ϵ''), dissipation factor ($\tan \Delta$) and real ac conductivity (σ'_{ac}) were investigated as a function of temperature (113- 293 K) and frequency (102- 106 Hz). The results clarified that all these dielectric parameters show a strong dispersion with temperatures at low and moderate frequency ranges. Moreover, they are strongly dependent on nano- Fe_2O_3 addition. Furthermore, the high content of nano- Fe_2O_3 addition ($x = 1.0$ wt. %) enhanced ϵ' and reduced $\tan D$ of ($\text{Cu}_{0.5}\text{Tl}_{0.5}$)-1223 phase, which is a desirable demand for practical applications.

Keywords

($\text{Cu}_{0.5}\text{Tl}_{0.5}$)-1223 phase, nano- Fe_2O_3 , electrical resistivity, dielectric constants.

1. INTRODUCTION

Among the currently known high temperature superconductors (HTSCs), $(\text{Cu}_{0.5}\text{Tl}_{0.5})\text{-1223}$ is one of the most promising candidates for technological applications. It has an amazing electrical properties such as; high superconducting transition temperature T_c , high ability to carry electrical currents and low anisotropy parameter (Ihara et al., 2000). Its structure consists of insulating $\text{Cu}_{0.5}\text{Tl}_{0.5}\text{Ba}_2\text{O}_{4-\delta}$ charge reservoir layer and three CuO_2 planes separated by Ca atoms (Ihara et al., 1997).

The complex dielectric constant ($\epsilon^* = \epsilon' + j\epsilon''$) originates from different polarization mechanisms. There are four primary mechanisms of polarization in materials; (a) electronic polarization, (b) atomic and ionic polarization, (c) dipolar or oriental polarization, and (d) interfacial or space charge polarization. Each mechanism involves a short range motion of charges and contributes to the total polarization of the material. The electronic polarization is observed at very high frequency of the order of $\sim 10^{15}$ Hz (i.e. in the ultraviolet optical range) and the atomic and ionic polarization takes place at frequencies in the infrared range of 10^{10} to 10^{13} Hz. The dipolar or oriental polarization occurs in the sub-infrared range of frequencies 10^3 to 10^6 Hz and the space charge or interfacial polarization is more sensitive in the low frequency range of 10^3 Hz and may extend to a few kilohertz range (Hench & West, 1990).

It has been observed that several cuprate superconductors have relatively high dielectric constants (Çavdar, Koralay, Tuğluoğlu, & Günen, 2005)-(Mohammed, 2012). The high dielectric constants are necessarily needed in many microelectronics applications, such as; capacitors and memory devices in modern computers. However, the obstacle for potential applications is the high dc conductivity, which results in a high dissipation loss. In this work, we survey the dielectric properties of $\text{Cu}_{0.5}\text{Tl}_{0.5}\text{Ba}_2\text{Ca}_2\text{Cu}_3\text{O}_{10-\delta}$ superconducting phase. This phase has an extremely high dielectric constant due to its layered structure along c-axis and modulated structure along a and b axes, making a possible nature internal barrier layer capacitors (IBLC) structure in the three dimensions. The charge reservoir layer, $\text{Cu}_{0.5}\text{Tl}_{0.5}\text{Ba}_2\text{O}_{4-\delta}$, of this phase localizes the charges at Tl^{+3} , Cu^{+2} and Ba^{+2} , whereas the CuO_2 planes contain mobile carriers, which get displaced by applying the external field. Most importantly, the dc conductivity of this phase, and in turn the dissipation loss, can be adjusted to a relatively low value by using high content of nano- Fe_2O_3 addition. As a result, high dielectric constant with relatively small dissipation loss was obtained at low and moderate frequency ranges in the titled phase.

2. EXPERIMENTAL TECHNIQUE

Superconducting samples of the nominal compositions $\text{Cu}_{0.5}\text{Tl}_{0.5}\text{Ba}_2\text{Ca}_2\text{Cu}_3\text{O}_{10-\delta}$ were prepared by a single step solid-state reaction technique. High purity oxides of Tl_2O_3 , BaO , CaO and CuO , taken in stoichiometric ratios 0.5: 2: 2: 3.5, were ground in agate mortar and sifted by a 65 μm sieve. Nano- Fe_2O_3 (Sigma Aldrich, particle size 20- 50 nm) was added to the sifted powder and well mixed to ensure the homogeneity of nano- Fe_2O_3 inside the sifted powder. The powder was pressed into a disc (diameter of 1.5 cm and thickness of about 0.3 cm), and then it was wrapped in a silver foil to minimize the thallium losses during the sintering process. The samples were heated in a sealed quartz tube (1.8 cm diameter and 12 cm long) at a rate of 20C/min to 760oC, followed by a rate of 10C/min to 850oC, and finally held at this temperature for five hours. Then, the samples were slowly cooled to room temperature by a rate of 4o/min.

The samples were characterized by X-ray powder diffraction (XRD) using Shimadzu-7000 XRD with $\text{CuK}\alpha$ -radiation ($\lambda = 1.5418 \text{ \AA}$) in the range $20^\circ \leq 2\theta \leq 70^\circ$. The microstructure morphology of the samples was identified using Jeol scanning electron microscope JSM-5300, operated at 25-30 kV, with a resolution power of 4 nm. Energy dispersive X-ray (EDX) analysis was performed for the prepared samples using Oxford X-ray micro-probe analyzer connected to Jeol scanning microscope JSM-5300.

The electrical resistivity of the prepared samples was measured by the conventional four-probe technique from room temperature down to T_0 via a closed cryogenic refrigeration system (Displex) employing helium gas as a working medium. The samples had the shape of parallelepipeds of approximate dimensions $1.5 \times 0.2 \times 0.3 \text{ cm}^3$. Copper leads were attached to the sample using a conductive silver paint.

The temperature of the sample was monitored by a chromel versus Fe-Au thermocouple and stabilized with the aid of a temperature controller to within ± 0.1 K. A low dc electric current, typically 1mA, is applied through the sample by Keithley-225 current source to avoid heating effects on the samples. The potential drop across the sample was measured using a Keithley-181 digital nano-voltmeter.

The capacitance (C_p) and conductance (G) of the studied samples were measured using HIOKI 3532-50 LCR HiTESTER in frequency and temperature ranges of 102- 106 Hz and 113-293 K, respectively. Room temperature curing silver paint was applied to both surfaces of a rectangular shaped sample with dimension of about $1.5 \times 0.4 \times 0.3$ cm³ and the specimen was left to dry at room temperature. A thin copper leads were fixed to the silver electrode surfaces and the conventional two probe technique was used. The dielectric constants (ϵ' and ϵ''), dissipation factor ($\tan \Delta$) and ac conductivity (σ'_{ac}) are related to the capacitance (C_p) and conductance (G) by the following relations:

$$\epsilon' = \frac{C_p d}{\epsilon_0 A}, \tag{1}$$

$$\epsilon'' = \frac{G d}{\epsilon_0 \omega A}, \tag{2}$$

$$\tan \Delta = \frac{\epsilon''}{\epsilon'}, \tag{3}$$

$$\sigma'_{ac} = \epsilon_0 \omega \epsilon' \tan \Delta, \tag{4}$$

where $\omega = 2 \pi f$ and f is the frequency of the applied ac field (Hz), d is the sample thickness (m), ϵ_0 is the permittivity of free space (8.85×10^{-12} F/m) and A is the area of the sample (m²).

3. RESULTS AND DISCUSSION

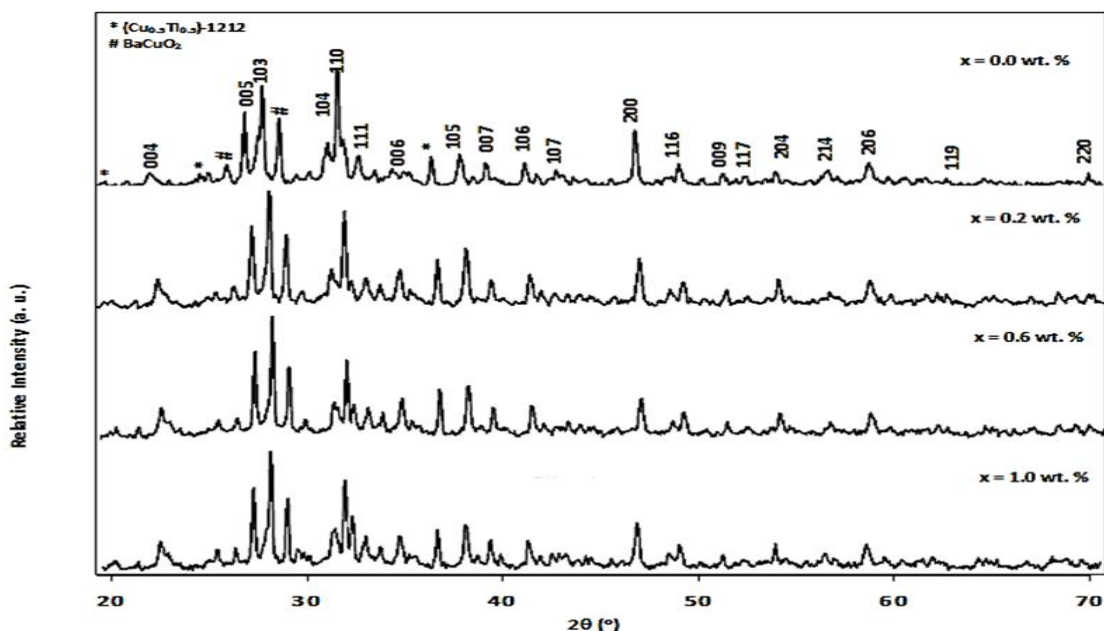


Fig.1: XRD patterns for $(\text{Fe}_2\text{O}_3)_x\text{Cu}_{0.5}\text{Tl}_{0.5}\text{Ba}_2\text{Ca}_2\text{Cu}_3\text{O}_{10-\delta}$ with $x = 0.0, 0.2, 0.6$ and 1.0 wt. %.

Room temperature XRD patterns of $(\text{Fe}_2\text{O}_3)_x\text{Cu}_0.5\text{Tl}_0.5\text{Ba}_2\text{Ca}_2\text{Cu}_3\text{O}_{10-\delta}$, where $x = 0.0, 0.2, 0.6$ and 1.0 wt. %, are displayed in Fig. 1. The XRD analysis indicates that the samples are mainly composed of $(\text{Cu}_0.5\text{Tl}_0.5)$ -1223 phase with tetragonal structure and $P4/mmm$ symmetry. Small amounts of secondary phases were detected, such as $(\text{Cu}_0.5\text{Tl}_0.5)$ -1212 and BaCuO_2 . It should be mentioned that there is no peaks corresponding to Fe_2O_3 or Fe-based compounds were detected in the XRD patterns. However, the EDX analysis (see Fig. 2) of $(\text{Fe}_2\text{O}_3)_x\text{Cu}_0.5\text{Tl}_0.5\text{Ba}_2\text{Ca}_2\text{Cu}_3\text{O}_{10-\delta}$ with $x = 0.2$ wt. % shows the existence of Fe element in the bulk sample. This means that nano- Fe_2O_3 does not enter the structure of the phase, but just occupies interstitial places between the grains. Similar results were observed by Annabi et al. (Annabi, M'Chirgui, Ben Azzouz, Zouaoui, & Ben Salem, 2004) for (Bi, Pd) -2223 superconducting phase added with nano- Al_2O_3 .

The volume fractions, for all the prepared samples, of $(\text{Cu}_0.5\text{Tl}_0.5)$ -1223, $(\text{Cu}_0.5\text{Tl}_0.5)$ -1212 and BaCuO_2 phases are calculated using all the peak intensities (Karaca, elebi, Varilci, & Malik, 2002) and their values are listed in Table 1. It is obvious that the volume fraction of $(\text{Cu}_0.5\text{Tl}_0.5)$ -1223 phase increases from 85.7 to 89.7 % as x increases from 0.0 to 0.2 wt. % afterwards, there is a retardation in its value for $x > 0.2$ wt. %. Similar results were reported for $(\text{Cu}_0.25\text{Tl}_0.75)$ -1234 and Bi -2223 phase added with nano- MgO (Awad, 2008) and nano- SnO_2 (Awad, Abou-Aly, Abdel Gawad, & G-Eldeen, 2012), respectively. They have assigned the decrease in the volume fraction for higher nano-oxide additions to the ability of solid nano-oxides to prevent, to some extent, the spatial phase growth. These results contradicted with those found by Yahya et al. (Yahya, (2004)) for Bi -2223 added with nano- Fe_2O_3 . The enhancement rate of volume fraction of $(\text{Cu}_0.5\text{Tl}_0.5)$ -1223 added with nano- Fe_2O_3 is 4.6 %, while the retardation rate is 1.6 %. This enhancement rate is greater than that found in our previous studies (Mohammed, Abou-Aly, Ibrahim, Awad, & Rekaby, 2011; Mohammed et al., 2012) for $(\text{Cu}_0.5\text{Tl}_0.5)$ -1223 added with nano- SnO_2 and nano- In_2O_3 . This indicates that the low addition of nano- Fe_2O_3 ($x = 0.2$ wt. %) is very significant in affecting the viscosity of the transient liquid forming at the reaction temperature, its homogeneity and the formation rate of the $(\text{Cu}_0.5\text{Tl}_0.5)$ -1223 phase (Ghattas, Annabi, Zouaoui, Azzouz, & Salem, 2008).

Table 1: Variation of volume fraction percentages and lattice parameters of $(\text{Cu}_{0.5}\text{Tl}_{0.5})$ -1223 with nano- Fe_2O_3 addition x

x (wt. %)	Volume fraction percentages		
	$(\text{Cu}_{0.5}\text{Tl}_{0.5})$ -1223 %	$(\text{Cu}_{0.5}\text{Tl}_{0.5})$ -1212 %	BaCuO_2 %
0.0	85.7	2.00	12.2
0.1	88.9	1.64	9.46
0.2	89.7	1.64	8.56
0.4	88.0	1.80	10.2
0.6	86.2	1.80	12.0
1.0	84.7	2.90	12.4

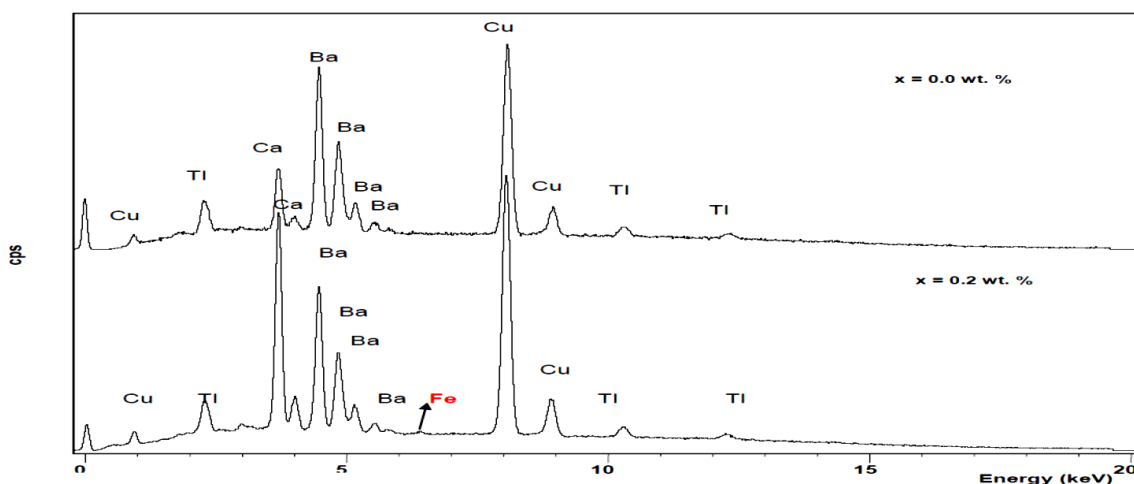


Fig.2: Typical EDX spectrum for $(\text{Fe}_2\text{O}_3)_x\text{Cu}_0.5\text{Tl}_0.5\text{Ba}_2\text{Ca}_2\text{Cu}_3\text{O}_{10-\delta}$ with $x = 0.0$ and 0.2 wt. %.

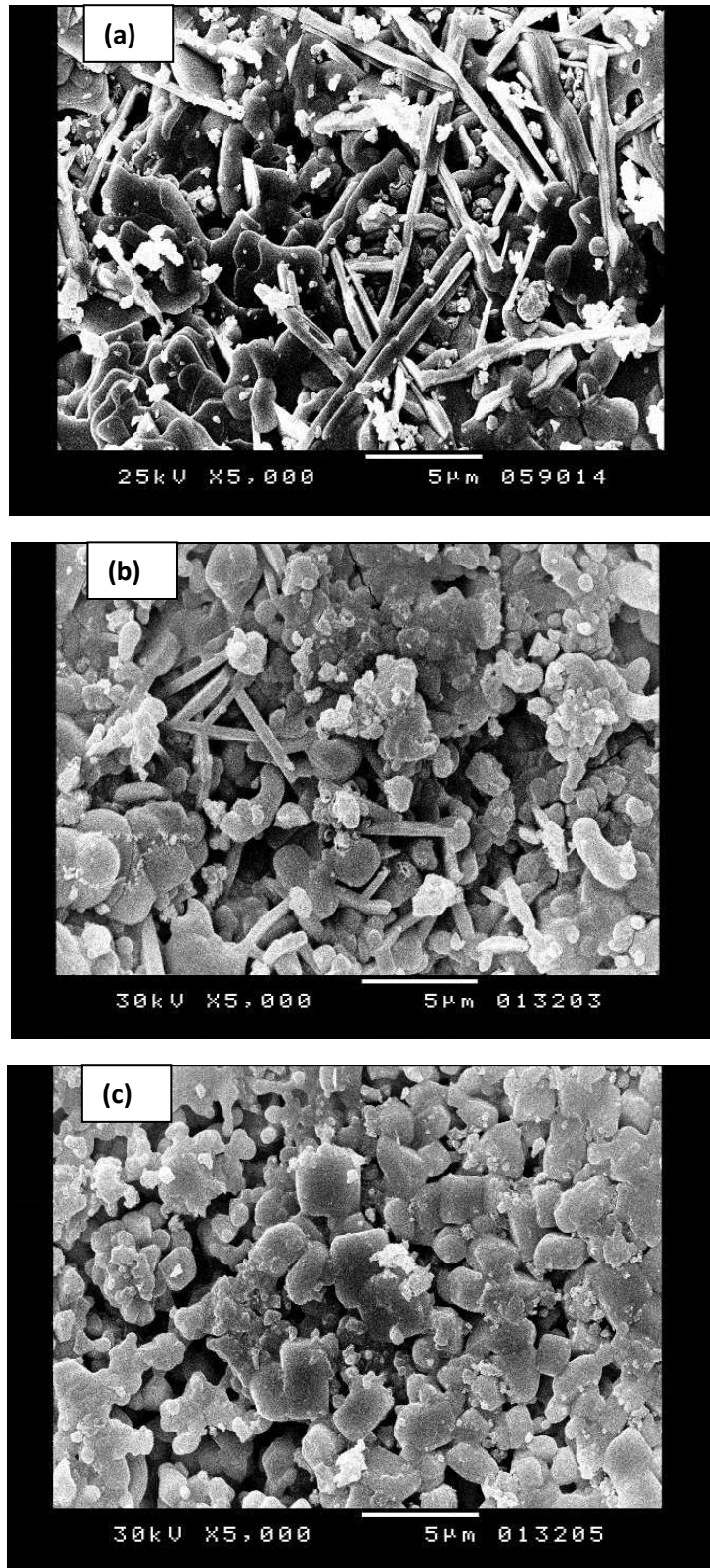


Fig.3: SEM micrographs for $(\text{Fe}_2\text{O}_3)_x\text{Cu}_{0.5}\text{Tl}_{0.5}\text{Ba}_2\text{Ca}_2\text{Cu}_3\text{O}_{10-\delta}$:
(a) $x = 0.0$ wt. %, (b) $x = 0.2$ wt. %, (c) $x = 0.6$ wt. %.

SEM micrographs for $(\text{Fe}_2\text{O}_3)_x\text{Cu}_0.5\text{Tl}_0.5\text{Ba}_2\text{Ca}_2\text{Cu}_3\text{O}_{10-\delta}$, $x = 0.0, 0.2$ and 0.6 wt. %, are shown in Figs. 3(a) to 3(c), respectively. It is clear that the morphology of the sample with $x = 0.0$ wt.%, consists of randomly oriented plate-like grains, indicating the formation of $(\text{Cu}_0.5\text{Tl}_0.5)$ -1223 phase. Badica et al. (Badica, Iyo, Crisan, & Ihara, 2002) found similar grains morphology for (Cu,Tl) -1234 phase. Also, it is clear that there is a little number of irregular shaped and spherical grains embedded between the plate-like grains of $(\text{Cu}_0.5\text{Tl}_0.5)$ -1223 phase. These irregular shaped and spherical grains may correspond to the impurity phases such as $(\text{Cu}_0.5\text{Tl}_0.5)$ -1212 and BaCuO_2 , respectively (Badica et al., 2002). Figs. 3(b) and 3(c) reveal that the addition of nano- Fe_2O_3 homogenously decreases the pores and weak links between the grains. Moreover, the addition of nano- Fe_2O_3 converts the plate-like grains to small well connected rectangular grains (Fig. 3(c)). This grain conversion increases the microstructure density of the prepared samples. Yahya et al. (Yahya, (2004))have reported similar effect for nano- Fe_2O_3 addition on grain morphology of Bi-2223 phase. They found that nano- Fe_2O_3 addition converted the randomly oriented grains with large number of weak links, of the pure sample, to a stacking up layers for nano- Fe_2O_3 addition equals to 0.01 g. It is clear from Figs. 3(b) and 3(c) that there are fine grains that may indicate the existence of nano- Fe_2O_3 in $(\text{Cu}_0.5\text{Tl}_0.5)$ -1223 matrix even after sintering at high temperatures. A similar fine alumina nanoparticles in the Y-211 matrix was found by Moutalibi et al. (Moutalibi, M'chirgui, & Noudem, 2010).

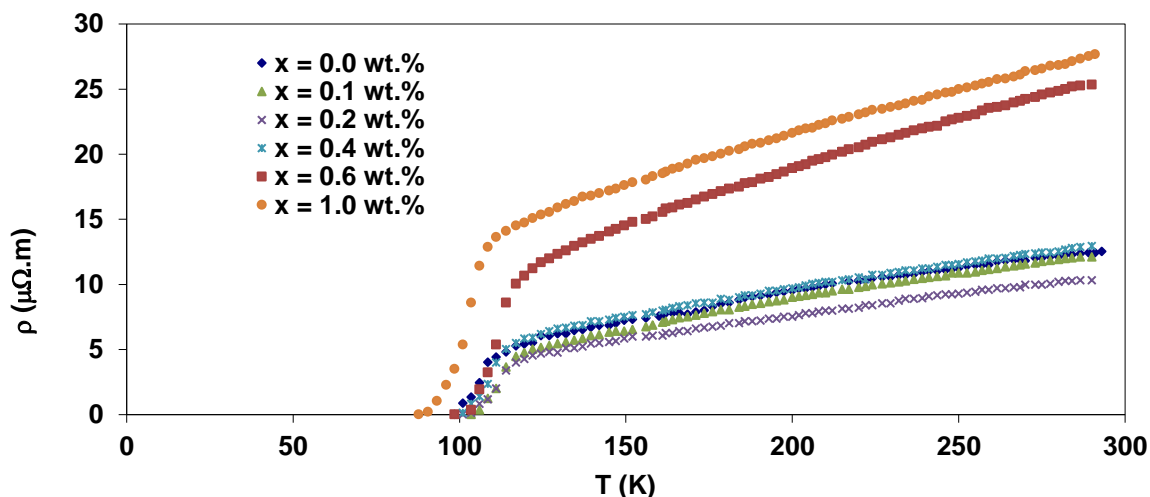


Fig.4: Temperature dependence of electrical resistivity for $(\text{Fe}_2\text{O}_3)_x\text{Cu}_0.5\text{Tl}_0.5\text{Ba}_2\text{Ca}_2\text{Cu}_3\text{O}_{10-\delta}$ with $x = 0.0, 0.1, 0.2, 0.4, 0.6$ and 1.0 wt. %.

The temperature dependence of the electrical resistivity for $(\text{Fe}_2\text{O}_3)_x\text{Cu}_0.5\text{Tl}_0.5\text{Ba}_2\text{Ca}_2\text{Cu}_3\text{O}_{10-\delta}$ with $x = 0.0, 0.1, 0.2, 0.4, 0.6$ and 1.0 wt. % is shown in Fig. 4. All the samples show metallic-like behavior above T_c and exhibit a transition to the superconducting state below T_c . A small curvature above T_c is observed, which is a characteristic of superconducting thermodynamic fluctuations (Abou-Aly, Awad, Ibrahim, & Abdeen, 2009). Generally, T_c is determined from the derivative of $\rho(T)$ with respect to T and the maximum of $d\rho(T)/dT$ corresponds to T_c (Salamati & Kameli, 2003). The variation of T_c with x for $(\text{Fe}_2\text{O}_3)_x\text{Cu}_0.5\text{Tl}_0.5\text{Ba}_2\text{Ca}_2\text{Cu}_3\text{O}_{10-\delta}$ is listed in table 2. It is obvious that T_c increases from 106 to 114 K as x varies from 0.0 to 0.2 wt. %, then it decreases for $x > 0.2$ wt. %. The suppression of T_c for $x > 0.2$ wt. % added nano- Fe_2O_3 may be due to the Cooper pair breaking mechanism (Barik, Ghorai, Bhattacharya, Kilian, & Chaudhuri, 2000). The T_c enhancement rate for $(\text{Fe}_2\text{O}_3)_x\text{Cu}_0.5\text{Tl}_0.5\text{Ba}_2\text{Ca}_2\text{Cu}_3\text{O}_{10-\delta}$ is 7.5 % while the retardation rate is 2.7 %. This enhancement rate is smaller than that obtained by Mohammed et al. (Mohammed et al., 2011) and Abou-Aly et al. (Abou-Aly, Abdel Gawad, Awad, & G-Eldeen, 2011) for $(\text{Cu}_0.5\text{Tl}_0.5)$ -1223 and (Bi,Pb) -2223, respectively, added with nano- SnO_2 . However, it is greater than that found for $(\text{Cu}_0.5\text{Tl}_0.5)$ -1223 added with nano- In_2O_3 (Mohammed, 2012).

Table 2: Variation of T_c , normal state resistivity ρ_n and residual resistivity ρ_0 with nano- Fe_2O_3 addition x

x (wt. %)	T_c (K)	ρ_n ($\square\square.m$)	ρ_0 ($\square\square.m$)
0.0	106	12.51	1.66
0.1	113	12.11	0.66
0.2	114	10.32	0.42
0.4	111	12.93	1.68
0.6	109	20.33	2.54
1.0	104	27.67	7.21

The normal state resistivity ρ_n and residual resistivity ρ_0 for $(\text{Fe}_2\text{O}_3)_x\text{Cu}_0.5\text{Tl}_0.5\text{Ba}_2\text{Ca}_2\text{Cu}_3\text{O}_{10-\delta}$ as a function of nano- Fe_2O_3 addition are listed in Table 2. Here ρ_n is the resistivity at room temperature and ρ_0 is obtained from the fitting of resistivity data in the temperature range $140\text{K} \leq T \leq 300\text{K}$ according to Matthiessen's rule (Abou-Aly et al., 2009). It is evident that both ρ_n and ρ_0 are decreased as x increases from 0.0 to 0.2 wt. % then they increase for $x > 0.2$ wt. %. These results are consistent with volume fraction as well as T_c calculations. Since the normal state resistivity is regarded as a measure of disorder; the disorder decreases for samples with lower nano- Fe_2O_3 addition ($x \leq 0.2$ wt. %) (Haugan et al., 2000). It is well known that the residual resistivity arises from the impurity scattering in the CuO_2 -plane. So, the decrease in ρ_0 for samples with $x \leq 0.2$ wt. % implies that the impurity scattering in the CuO_2 -plane also decreases.

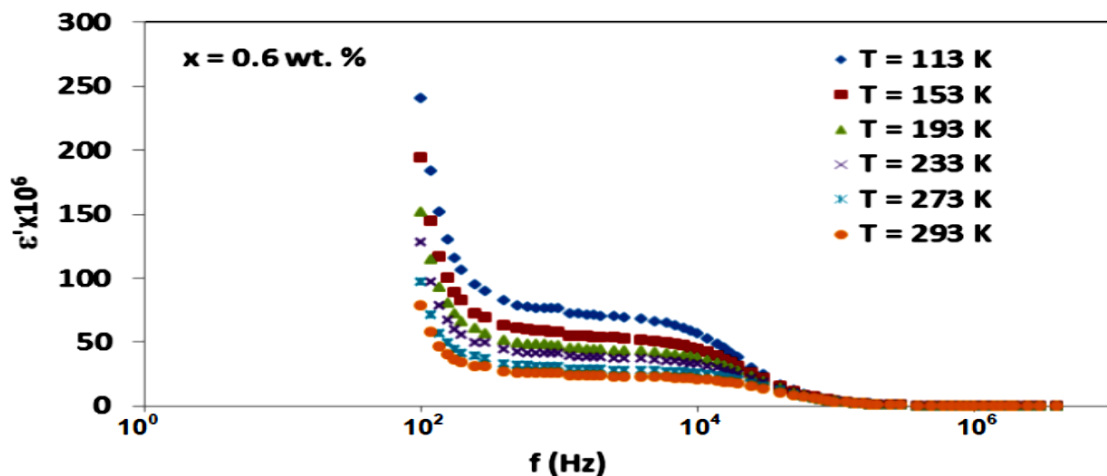


Fig.5: Frequency dependence of ϵ' at different temperatures for $(\text{Fe}_2\text{O}_3)_x\text{Cu}_0.5\text{Tl}_0.5\text{Ba}_2\text{Ca}_2\text{Cu}_3\text{O}_{10-\delta}$ with $x = 0.6$ wt. %.

Fig. 5 shows the frequency dependence of the real dielectric constant ϵ' at different temperatures ($T = 113, 153, 193, 233, 273$ and 293 K) for $(\text{Fe}_2\text{O}_3)_x\text{Cu}_0.5\text{Tl}_0.5\text{Ba}_2\text{Ca}_2\text{Cu}_3\text{O}_{10-\delta}$ with $x = 0.6$ wt. %. In general, the sample demonstrates distinct behaviors at different frequency ranges and the values of ϵ' are found to be extremely high ≥ 106 . In the low frequency range (102-103Hz), ϵ' starts by a highest value at $f = 102$ Hz and $T = 113$ K then shifts gradually to lower values with increasing both frequency and temperature. These extremely high ϵ' values are attributed to interfacial polarization that occurs mainly in low frequency range (Krohns, (2008)). Interfacial polarization can occur: (a) externally at the surface of the sample due to the formation of a Schottky diode at the electrode/sample contact (Lunkenheimer, Fichtl, Ebbinghaus, & Loidl, 2004) and/or (b) internally from grain boundaries in ceramic samples or planar crystal defects such as twin boundaries (Sinclair, (2002)). Moreover, the layered structure of the phase gives it possible nature internal barrier layer capacitors (IBLC) structure in the three dimensions. All these sources of interfacial polarization could generate extremely high values of the dielectric constant.

As the frequency increases from 103 to 104 Hz, the interfacial polarization is relaxed and the first plateau region is reached, where ϵ' becomes invariant with frequency. This is because the available time for drifting the charge carriers is reduced and the observed high values of ϵ' is substantially lowered. In this case the polarizability is associated with the bulk material rather than the interface. With further increase in f (104-105 Hz), a step-like decrease in ϵ' with increasing frequency is observed. This type of relaxation is always a clear sign for dipolar polarization which occurs when the frequency of the outer applied electric field ($f = \omega/2\pi$) corresponds to reorientation times of molecular dipoles. This kind of polarization may originate from the presence of permanent orientable dipoles or dipolar effects that caused by impurities, lattice defects or the presence of charge carriers (Xu et al., 2005). Near the end of this frequency range, the oscillation of the applied field is too fast and the dipolar polarization characteristic time is longer than the time constant of the applied field (Mumtaz & Khan, 2009). So the contribution to polarization from dipolar mechanism ceased. Beyond 105 Hz, a second plateau region is reached, where ϵ' becomes both frequency and temperature independent.

The measured values of ϵ' are found to be two order of magnitude greater than those reported for $\text{YBa}_2\text{Cu}_3\text{O}_{7-\delta}$ (Rey, Mathias, Testardi, & Skirius, 1992), $\text{PrBa}_2\text{Cu}_3\text{O}_7$ (Cao, O'Reilly, Crow, & Testardi, 1993), $\text{La}_2\text{Cu}_3\text{O}_4$ (Mazzara et al., 1993), Gd_2CuO_4 (Shi, 1998), Bi_2CuO_4 (Yoshii et al., 2011) and Nd_2CuO_4 (Chen, Wang, & Chen, 1997). Also, they are one order of magnitude smaller than those reported for MgB_2 (Cui, Zhang, & Wang, 2006). However, they are comparable with those found for $\text{CaCu}_3\text{Ti}_4\text{O}_{12}$ (Yua, (2005)).

On the other hand, Mumtaz and Khan (Mumtaz & Khan, 2009) studied the dielectric properties of $\text{Cu}_{0.5}\text{Tl}_{0.5}\text{Ba}_2\text{Ca}_{2-y}\text{Mg}_y\text{Cu}_{0.5}\text{Zn}_{2.5}\text{O}_{10-\delta}$ ($y = 0.0, 0.5, 1.0$ and 1.5) and $\text{Cu}_{0.5}\text{Tl}_{0.5}\text{Ba}_2\text{Ca}_3\text{Cu}_4\text{O}_{12-\delta}$ superconductors in the range of 10 KHz to 10 MHz. They observed a negative capacitance (NC) phenomenon. A similar NC phenomenon was also observed by Cavdar et al. (Cavdar et al., 2005) for Tl-2212 and Tl-2223 phases.

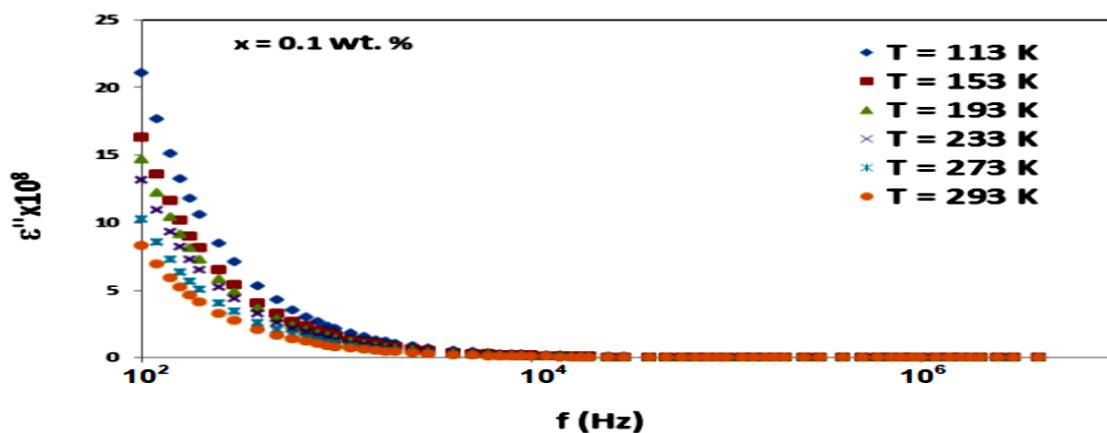


Fig.6: Frequency dependence of ϵ'' at different temperatures for $(\text{Fe}_2\text{O}_3)_x\text{Cu}_{0.5}\text{Tl}_{0.5}\text{Ba}_2\text{Ca}_2\text{Cu}_3\text{O}_{10-\delta}$ with $x = 0.1$ wt. %.

Fig. 6 displays the frequency dependence of the imaginary dielectric constant ϵ'' at different temperatures ($T = 113, 153, 193, 233, 273$ and 293 K) for $(\text{Fe}_2\text{O}_3)_x\text{Cu}_{0.5}\text{Tl}_{0.5}\text{Ba}_2\text{Ca}_2\text{Cu}_3\text{O}_{10-\delta}$ with $x = 0.1$ wt. %. The imaginary dielectric constant arises due to the lag in polarization with the applied ac-field (Mumtaz & Khan, 2009). It is clear that ϵ'' decreases with the increase of frequency and temperature. High dispersion characteristics are observed in the ϵ'' curves at frequencies lower than 1 kHz. This could be attributed due to the interfacial polarization. The degree of dispersion decreases as the frequency increases. In the frequency range of 10-103 kHz, a frequency independent response is observed over the entire temperature range studied. This may be attributed due to the inherent characteristic of dielectric materials as the oscillating system cannot follow the resonant frequency in an applied field. The phenomenon of dielectric dispersion could be explained on the basis of Koops phenomenological theory (Koops, 1951) of dielectrics. In this model, a dielectric medium has been assumed to be made of well conducting grains, which are separated by poorly conducting grain boundaries.

Therefore the grains are highly conductive and have high values of permittivity, while the grain boundaries are less conductive and have smaller values of permittivity. At lower frequencies the grain boundaries are more effective than electrical conduction grains. Also, it should be mentioned that there is no peak appeared in ϵ'' curve. Usually, this peak appears at characteristic frequency corresponding to the step-like decrease of ϵ' and it suggests the presence of relaxing dipoles in the samples. Similar behavior was reported by Çavdar et al. (Çavdar et al., 2005) for Tl-2212 and Tl-2223 phases and by Verma et al. (Verma, Goel, Mendiratta, & Alam, 1999) for NiZn ferrites.

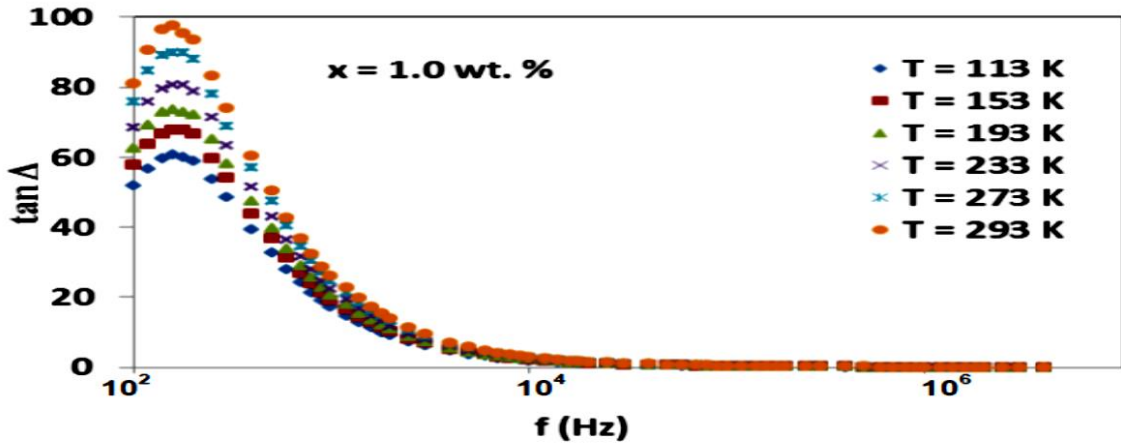


Fig.7: Frequency dependence of $\tan \Delta$ at different temperatures for $(\text{Fe}_2\text{O}_3)_x\text{Cu}_{0.5}\text{Tl}_{0.5}\text{Ba}_2\text{Ca}_2\text{Cu}_3\text{O}_{10-\delta}$ with $x = 1.0$ wt. %.

Fig.7 shows the frequency dependence of $\tan \Delta$ at different temperatures ($T = 113, 153, 193, 233, 273$ and 293 K) for $(\text{Fe}_2\text{O}_3)_x\text{Cu}_{0.5}\text{Tl}_{0.5}\text{Ba}_2\text{Ca}_2\text{Cu}_3\text{O}_{10-\delta}$ with $x = 1.0$ wt. %. It is clear that $\tan \Delta$ decreases with the increase of frequency. At the low frequency range it shows a peak, corresponding to the abrupt decrease of ϵ' . Also, it is obvious that the peak position does not alter with temperature variation. This result is in contrast with Wu et al. (Wu, Nan, Lin, & Deng, 2002) and Xu et al. (Xu et al., 2005). They found that the peak's position shifts towards lower frequency with decreasing temperature, and they explained such dielectric response by a Debye-like relaxation process. Moreover, very high values of $\tan \Delta$ are observed at low frequencies. At higher frequencies $\tan \Delta$ exponentially decreases to lower values. These high $\tan \Delta$ values result from the dielectric losses, which are mainly due to the relatively high dc conductivities of the prepared samples.

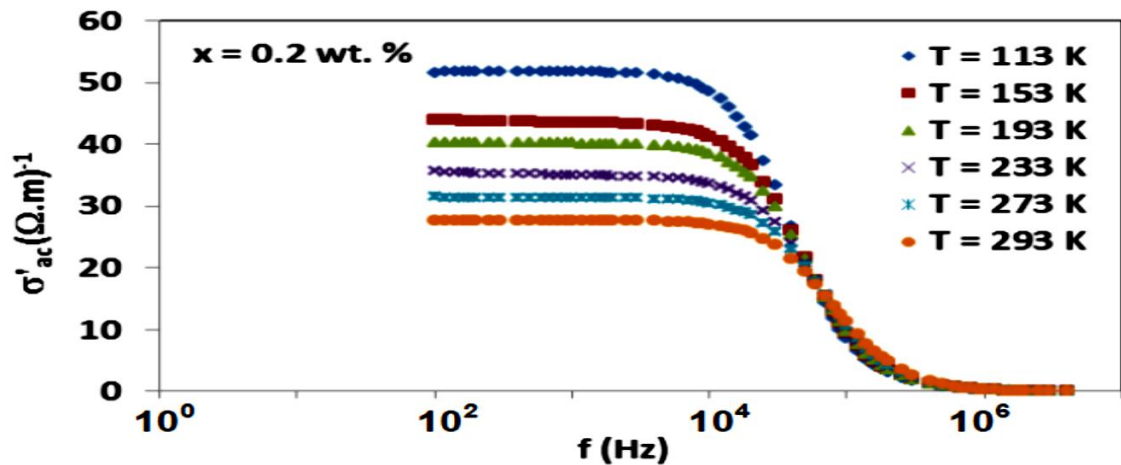


Fig. 8: Frequency dependence of σ'_{ac} at different temperatures for $(\text{Fe}_2\text{O}_3)_x\text{Cu}_{0.5}\text{Tl}_{0.5}\text{Ba}_2\text{Ca}_2\text{Cu}_3\text{O}_{10-\delta}$ with $x = 0.2$ wt. %.

Table 3: Variation of frequency exponent s with T for (Fe₂O₃)_xCu_{0.5}Tl_{0.5}Ba₂Ca₂Cu₃O_{10-δ}

s-values						
T(K)	x = 0.0 wt. %	x = 0.1 wt. %	x = 0.2 wt. %	x = 0.4 wt. %	x = 0.6 wt. %	x = 1.0 wt. %
113	0.97	0.58	0.74	0.69	0.66	0.44
153	0.84	0.50	0.60	0.58	0.56	0.41
193	0.81	0.37	0.54	0.53	0.49	0.33
233	0.79	0.31	0.45	0.47	0.44	0.29
273	0.78	0.21	0.39	0.41	0.36	0.25
293	0.77	0.17	0.32	0.34	0.31	0.23

Fig. 8 shows the frequency dependence of the real ac conductivity σ'_{ac} at different temperatures ($T = 113, 153, 193, 233, 273$ and 293 K) for $(\text{Fe}_2\text{O}_3)_x\text{Cu}_{0.5}\text{Tl}_{0.5}\text{Ba}_2\text{Ca}_2\text{Cu}_3\text{O}_{10-\delta}$ with $x = 0.2$ wt. %. It is clear that there is a frequency independent plateau appears in the low frequency region (102-104 Hz), while at higher frequencies σ'_{ac} starts to decrease with increasing frequency. This dependence of σ'_{ac} on frequency can be expressed by the following relation (Shi, 1998):

$$\sigma'_{ac}(\omega) = \sigma_{dc} + \sigma_{ac}, \quad (5)$$

where σ_{dc} is a frequency independent term represent the dc electric conductivity which is related to the drift mobility of the free charge carriers and σ_{ac} is a frequency dependent term which is related to the dielectric relaxation of the bound charger carriers. σ_{dc} is predominant at low frequencies, while σ_{ac} is predominant at high frequencies. The frequency dependence of the second term σ_{ac} can be written as

$$\sigma_{ac} = Q\omega^{-s}, \quad (6)$$

where Q is the pre-exponential factor and s is the frequency exponent with values between 0 and 1. The values of s in equation (6) were extracted from the slopes of the plots of $\ln \sigma_{ac}$ versus $\ln \omega$ as shown in Fig. 9. The temperature dependence of s values was listed in Table 3. The temperature dependence of the real ac conductivity is studied by plotting $\ln \sigma'_{ac}$ versus $1000/T$ at $f = 1$ kHz and 100 kHz for $(\text{Fe}_2\text{O}_3)_x\text{Cu}_{0.5}\text{Tl}_{0.5}\text{Ba}_2\text{Ca}_2\text{Cu}_3\text{O}_{10-\delta}$, with $x = 0.4$ wt. %, as shown in Fig. 10. It is clear that σ'_{ac} decreases with increasing temperature and the decreasing rate is much higher at low frequency ($f = 1$ kHz) than that at high frequency ($f = 100$ kHz). This may indicate that the ac conductivity is a thermally activated process and can be analyzed according to the well known Arrhenius equation:

$$\sigma'_{ac} = \sigma^* e^{\frac{U}{k_B T}} \quad (7)$$

where σ^* is constant, U is the activation energy for conduction and k_B is Boltzmann constant. Due to the superconducting nature of the prepared samples, Arrhenius equation has a positive exponent. This behavior is opposite to the behavior of semiconductor materials (M. S. Hossain, (2008)), (Hendi, (2011)). Since, they have an ac conductivity increases exponentially with temperature.

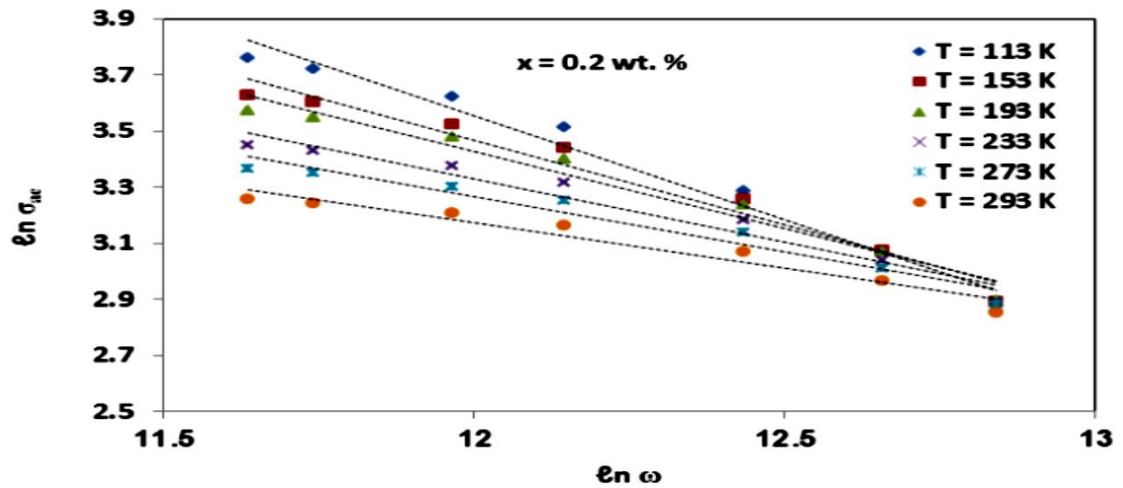


Fig.9: The plots of $\ln \sigma_{ac}$ versus $\ln \omega$ for $(Fe_2O_3)_xCu_{0.5}Tl_{0.5}Ba_2Ca_2Cu_3O_{10-\delta}$ with $x = 0.2$ wt. %.

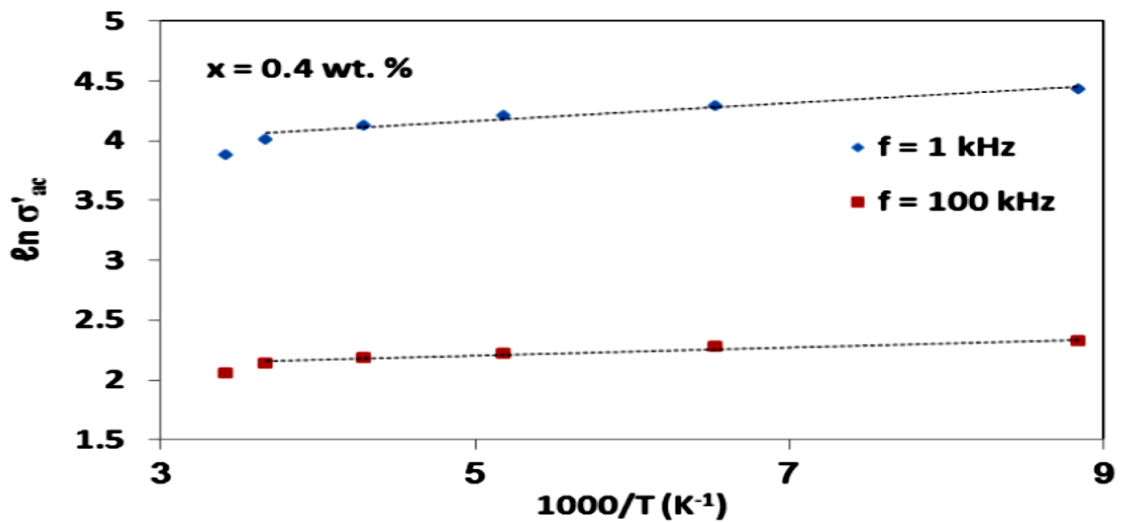


Fig.10: The plot of $\ln \sigma'_{ac}$ as a function of $1000/T$ at $f = 1$ and 100 kHz for $(Fe_2O_3)_xCu_{0.5}Tl_{0.5}Ba_2Ca_2Cu_3O_{10-\delta}$ with $x = 0.4$ wt. %.

Table 4: The calculated values of the activation energy for conduction U with x for $(Fe_2O_3)_xCu_{0.5}Tl_{0.5}Ba_2Ca_2Cu_3O_{10-\delta}$

U (eV)		
x (wt. %)	At f = 1 kHz	At f = 100 kHz
0.0	0.0052	0.0014
0.1	0.0110	0.0083
0.2	0.0079	0.0025
0.4	0.0064	0.0030
0.6	0.0070	0.0031
1.0	0.0058	0.0026

Table 5: Variation of ϵ' , ϵ'' , $\text{Tan } \Delta$ and σ'_{ac} with x at $f = 10^2\text{Hz}$ and $T = 113\text{ K}$ and 293 K for $(\text{Fe}_2\text{O}_3)_x\text{Cu}_{0.5}\text{Tl}_{0.5}\text{Ba}_2\text{Ca}_2\text{Cu}_3\text{O}_{10-\delta}$

f = 10² Hz and T = 113 K				
x (wt. %)	$\epsilon' \times 10^6$	$\epsilon'' \times 10^8$	Tan Δ	$\sigma'_{ac}(\Omega.m)^{-1}$
0.0	12.0	39.6	315	22.0
0.1	3.03	21.1	632	11.7
0.2	78.4	92.9	118	51.6
0.4	213	150	70.4	83.7
0.6	239	161	67.4	89.9
1.0	385	199	51.8	111
f = 10² Hz and T = 293 K				
0.0	6.64	30.3	424	16.8
0.1	0.23	8.2	2332	4.61
0.2	22.5	49.7	220	27.6
0.4	69.7	87.5	125	48.6
0.6	78.5	92.6	117	51.5
1.0	160	129	80.8	72.0

The activation energy of conduction, U , was calculated at $f = 1\text{ kHz}$ and 100 kHz from the slopes of the plots of $\ln \sigma'_{ac}$ versus $1000/T$. The calculated values are listed in Table 4. The values of U are comparable with those for $\text{CaCu}_3\text{Ti}_4\text{O}_{12}$ (Homes, Vogt, Shapiro, Wakimoto, & Ramirez, 2001) and much smaller than those of Bi-2222 (Xu et al., 2005). It can be seen that U decreases with increasing frequency. This is because the increase of the applied field frequency enhances electronic jumps between localized states and consequently the ac activation energy decreases with increasing frequency (Afifi, Bekheet, Abd Elwahhab, & Atyia, 2001).

The effect of nano- Fe_2O_3 addition on ϵ' , ϵ'' , $\text{Tan } \Delta$ and σ'_{ac} for $(\text{Fe}_2\text{O}_3)_x\text{Cu}_{0.5}\text{Tl}_{0.5}\text{Ba}_2\text{Ca}_2\text{Cu}_3\text{O}_{10-\delta}$, at $f = 102\text{ Hz}$ and $T = 113\text{ K}$ and 293 K , has been summarized and listed in Table 5. It is clear, for both selected temperatures, that nano- Fe_2O_3 addition decreases ϵ' till $x = 0.1\text{ wt. \%}$ then it increases for $x > 0.1\text{ wt. \%}$. Also, it is clear that sample with $x = 1.0\text{ wt. \%}$ has the highest recorded ϵ' value and the lowest recorded $\text{tan } \Delta$ value. This is because the large amount of nano- Fe_2O_3 addition causes degeneration of the main phase and growth of impurities, grain boundaries and secondary phases. This result is found to be consistent with relative volume fraction percentages calculations. Similar behavior for $\text{tan } \Delta$ variation with x is observed for $\text{Cu}_{0.5}\text{Tl}_{0.5}\text{Ba}_2\text{Ca}_2\text{-yMg}_y\text{Cu}_{0.5}\text{Zn}_{2.5}\text{O}_{10-\delta}$ ($y = 0, 0.5, 1.0, 1.5$) samples (Mumtaz & Khan, 2009). They found that with the increase of Mg substitution, the loss tangent consequently decreased at both room temperature (290 K) and 79 K . They attributed this behavior to the increase of carrier concentration in the conducting CuO_2 planes with the Mg substitution. Moreover, it is clear that ϵ'' and σ'_{ac} follow the same variation of ϵ' with x . Also, it can be seen that ϵ' , ϵ'' and σ'_{ac} values at $T = 113\text{ K}$, for all x values, are much higher than their values at $T = 293\text{ K}$ while $\text{tan } \Delta$ values at $T = 113\text{ K}$ are much lower than their values at $T = 293\text{ K}$. This may be attributed to that at low temperatures, close to the T_c of the prepared samples, transition from normal state to superconducting state starts and the samples acquire layered separated structures representing internal interfaces. At these internal interfaces charges can be blocked and give rise to interfacial polarization. However, as temperature increases, far from T_c , charges cannot be blocked anymore and ϵ' , ϵ'' and σ'_{ac} are reduced compared to their low temperature values at 113 K .

This behavior is contradicted with many other reports (Mazzara et al., 1993), (Rey et al., 1992), (Cao et al., 1993) which showed that ϵ' reached the highest values with increasing temperature. However, similar results were obtained by Cui et al. (Cui et al., 2006) for MgB_2 .

4. CONCLUSIONS

The effect of nano-Fe₂O₃ additions on the phase formation, microstructure, electrical resistivity and dielectric of (Cu_{0.5}Tl_{0.5})-1223 superconducting phase was studied. XRD indicated that (Cu_{0.5}Tl_{0.5})-1223 maintained its tetragonal structure even after nano-Fe₂O₃ additions. The electrical resistivity measurements indicated that the sample's T_c increased from 106 to 114 K as x was varied from 0.0 to 0.2 wt. %, and then it decreased as x increased. The retardation of T_c for x > 0.2 wt. % was attributed to Cooper pair breaking mechanism. The Dielectric measurements revealed that all the prepared samples have extremely high values of ϵ' ($\geq 10^6$) and this was attributed to interfacial polarization. It was found that sample with x = 1.0 wt. % added nano-Fe₂O₃ has the highest recorded values of ϵ'' and ϵ'_{ac} and the lowest values of $\tan \delta$ for the selected temperature T = 113 K and 293 K. This was attributed to the ability of high nano-Fe₂O₃ content to increase impurities, grain boundaries and secondary phases. This result is found to be consistent with relative volume fraction percentages calculation. The enhancement of ϵ' and the reduction of $\tan \delta$ for sample with nano-Fe₂O₃ addition equals to 1.0 wt. % is a desirable demand for practical applications.

Acknowledgments

This work was performed in Superconductivity and Metallic glasses laboratory, Physics Department, Faculty of Science, Alexandria University, Alexandria- Egypt.

REFERENCES

- Abou-Aly, A. I., Abdel Gawad, M. M. H., Awad, R., & G-Eldeen, I. (2011). Improving the Physical Properties of (Bi, Pb)-2223 Phase by SnO₂ Nano-particles Addition. *Journal of Superconductivity and Novel Magnetism*, 24(7), 2077.
- Abou-Aly, A. I., Awad, R., Ibrahim, I. H., & Abdeen, W. (2009). Effect of Sm-substitution on the electrical and magnetic properties of (Tl_{0.8}Hg_{0.2})-1223. *Journal of Alloys and Compounds*, 481(1), 462-469.
- Afifi, M. A., Bekheet, A. E., Abd Elwahhab, E., & Atyia, H. E. (2001). Ac conductivity and dielectric properties of amorphous In₂Se₃ films. *Vacuum*, 61(1), 9-17.
- Annabi, M., M'Chirgui, A., Ben Azzouz, F., Zouaoui, M., & Ben Salem, M. (2004). Addition of nanometer Al₂O₃ during the final processing of (Bi,Pb)-2223 superconductors. *Physica C: Superconductivity*, 405(1), 25-33.
- Awad, R. (2008). Study of the Influence of MgO Nano-Oxide Addition on the Electrical and Mechanical Properties of (Cu_{0.25}Tl_{0.75})-1234 Superconducting Phase. *Journal of Superconductivity and Novel Magnetism*, 21(8), 461-466.
- Awad, R., Abou-Aly, A. I., Abdel Gawad, M. M. H., & G-Eldeen, I. (2012). The Influence of SnO₂ Nano-Particles Addition on the Vickers Microhardness of (Bi, Pb)-2223 Superconducting Phase. *Journal of Superconductivity and Novel Magnetism*, 25(4), 739-745.
- Badica, P., Iyo, A., Crisan, A., & Ihara, H. (2002). (Cu,Tl)Ba₂Ca₃Cu₄O_x compositions: II. Heating rate applied to synthesis of superconducting ceramics. *Superconductor Science and Technology*, 15(6), 975-982.
- Barik, H. K., Ghorai, S. K., Bhattacharya, S., Kilian, D., & Chaudhuri, B. K. (2000). Effect of Cr doping on the electrical conductivity and Seebeck coefficient in the superconductors obtained from the Bi–Pb–Sr–Ca–Cu–Cr–O-type glassy precursors by annealing. *Journal of Materials Research*, 15(5), 1076-1082.
- Cao, G., O'Reilly, J. W., Crow, J. E., & Testardi, L. R. (1993). Enhanced electric polarizability at the magnetic ordering temperature of La₂CuO_{4+x}. *Physical Review B*, 47(17), 11510.
- Çavdar, Ş., Koralay, H., Tuğluoğlu, N., & Günen, A. (2005). Frequency-dependent dielectric characteristics of Tl–Ba–Ca–Cu–O bulk superconductor. *Superconductor Science and Technology*, 18(9), 1204-1209.
- Chen, J. W., Wang, J. C., & Chen, Y. F. (1997). Study of dielectric relaxation behavior in Nd₂CuO₄. *Physica C: Superconductivity*, 289(1), 131-136.

- Cui, Y., Zhang, L., & Wang, R. (2006). Dielectric properties of polycrystalline MgB₂. *Physica C: Superconductivity and its Applications*, 442(1), 29-32.
- Ghattas, A., Annabi, M., Zouaoui, M., Azzouz, F. B., & Salem, M. B. (2008). Flux pinning by Al-based nano particles embedded in polycrystalline (Bi,Pb)-2223 superconductors. *Physica C: Superconductivity and its Applications*, 468(1), 31-38.
- Haugan, T., Wong-Ng, W., Cook, L. P., Brown, H. J., Swartzendruber, L., & Shaw, D. T. (2000). Flux pinning of Bi₂Sr₂CaCu₂O_{8+δ}/Ag superconductors utilizing (Sr,Ca)₁₄Cu₂₄O₄₁ defects and nanophase Al₂O₃ and Au particles. *Physica C: Superconductivity*, 335(1), 129-133.
- Hench, L. L., & West, J. K. (1990). *Principles of Electronic Ceramics*. John Wiley & Sons. New York..
- Hendi, A. A. ((2011)). Structure, Electrical Conductivity and Dielectric properties of bulk, 2-amino-(4,5-diphenylfuran-3-carbonitrile). *Life Science Journal*, 8(3) 554-559.
- Homes, C. C., Vogt, T., Shapiro, S. M., Wakimoto, S., & Ramirez, A. P. (2001). Optical Response of High-Dielectric-Constant Perovskite-Related Oxide. *Science*, 293(5530), 673.
- Ihara, H., Tanaka, K., Tanaka, Y., Iyo, A., Terada, N., Tokumoto, M., . . . Watanabe, T. (2000). Selective reduction for hole-doping in Cu_{1-x}Tl_x-1223 (Cu_{1-x}Tl_xBa₂Ca₂Cu₃O_{10-y}) system with T_c>132K. *Physica B: Condensed Matter*, 284-288, 1085-1086.
- Ihara, H., Tokiwa, K., Tanaka, K., Tsukamoto, T., Watanabe, T., Yamamoto, H., . . . Umeda, M. (1997). Cu_{1-x}Tl_xBa₂Ca₃Cu₄O_{12-y} (Cu_{1-x}Tl_x-1234) superconductor with T_c=126 K. *Physica C: Superconductivity*, 282-287, 957-958.
- Karaca, I., elebi, S., Varilci, A., & Malik, A. I. (2002). Effect of Ag₂O addition on the intergranular properties of the superconducting Bi (Pb) Sr Ca Cu O system. *Superconductor Science and Technology*, 16(1), 100-104.
- Koops, C. G. (1951). On the Dispersion of Resistivity and Dielectric Constant of Some Semiconductors at Audiofrequencies. *Physical Review*, 83(1), 121-124.
- Krohns, S., Lunkenheimer, P., Ebbinghaus, S. G., & Loidl, A. (2008). Colossal dielectric constants in single-crystalline and ceramic CaCu₃Ti₄O₁₂ investigated by broadband dielectric spectroscopy. *Journal of Applied Physics*, 103(8), 084107.
- Lunkenheimer, P., Fichtl, R., Ebbinghaus, S. G., & Loidl, A. (2004). Nonintrinsic origin of the colossal dielectric constants. *Physical Review B*, 70(17), 172102.
- Hossain, M. S., Islam, R., & Khan, K. A. (2008). Electrical conduction mechanisms of undoped and vanadium doped ZnTe thin films. *Chalcogenide Letters*, 5(1), 1-9.
- Mazzara, G. P., Skirius, S., Cao, G., Chern, G., Clark, R. J., Crow, J. E., ... & Testardi, L. R. (1993). High dielectric permittivity of ceramic and single-crystal PrBa₂Cu₃O_x. *Physical Review B*, 47(13), 8119.
- Mohammed, N. H. (2012). Effect of MgO Nano-oxide Additions on the Superconductivity and Dielectric Properties of Cu_{0.25}Tl_{0.75}Ba₂Ca₃Cu₄O_{12-δ} Superconducting Phase. *Journal of Superconductivity and Novel Magnetism*, 25(1), 45-53.
- Mohammed, N. H., Abou-Aly, A. I., Ibrahim, I. H., Awad, R., & Rekaby, M. (2011). Effect of Nano-Oxides Addition on the Mechanical Properties of (Cu_{0.5}Tl_{0.5})-1223 Phase. *Journal of Superconductivity and Novel Magnetism*, 24(5), 1463-1472.
- Mohammed, N. H., Awad, R., Abou-Aly, A. I., Ibrahim, I. H., Roumié, M., & Rekaby, M. (2012). Ion Beam Analysis and Electrical Resistivity Studies of (Cu_{0.5}Tl_{0.5})-1223 Phase with Added Nano-oxides. *Journal of Superconductivity and Novel Magnetism*, 25(5), 1441-1454.
- Moutalibi, N., M'chirgui, A., & Noudem, J. (2010). Alumina nano-inclusions as effective flux pinning centers in Y-Ba-Cu-O superconductor fabricated by seeded infiltration and growth. *Physica C: Superconductivity*, 470(13), 568-574.
- Mumtaz, M., & Khan, N. A. (2009). Dielectric response of Cu_{0.5}Tl_{0.5}Ba₂(Ca_{2-y}Mgy)(Cu_{0.5}Zn_{2.5})O_{10-δ} bulk superconductor to frequency and temperature. *Physica C: Superconductivity*, 469(4), 182-187.
- Rey, C. M., Mathias, H., Testardi, L. R., & Skirius, S. (1992). High dielectric constant and nonlinear electric response in nonmetallic YBa₂Cu₃O_{6+δ}. *Physical Review B*, 45(18), 10639.
- Salamati, H., & Kameli, P. (2003). Effect of deoxygenation on the weak-link behavior of YBa₂Cu₃O_{7-δ} superconductors. *Solid State Communications*, 125(7), 407-411.

- Shi, J. B. (1998). Dielectric studies in T* and T' structures of (La, Gd)₂CuO₄. *Physica C: Superconductivity*, 305(1), 35-45.
- Sinclair, D. C., Adams, T. B., Morrison, F. D., & West, A. R. (2002). CaCu₃Ti₄O₁₂: one-step internal barrier layer capacitor. *Applied Physics Letters*, 80(12), 2153-2155.
- Verma, A., Goel, T. C., Mendiratta, R. G., & Alam, M. I. (1999). Dielectric properties of NiZn ferrites prepared by the citrate precursor method. *Materials Science and Engineering: B*, 60(2), 156-162.
- Wu, J., Nan, C.-W., Lin, Y., & Deng, Y. (2002). Giant Dielectric Permittivity Observed in Li and Ti Doped NiO. *Physical Review Letters*, 89(21), 217601.
- Xu, X., Jiao, Z., Fu, M., Feng, L., Xu, K., Zuo, R., & Chen, X. (2005). Dielectric studies in a layered Ba based Bi-2222 cuprate Bi₂Ba₂Nd_{1.6}Ce_{0.4}Cu₂O_{10+δ}. *Physica C: Superconductivity*, 417(3), 166-170.
- Yahya, S. Y., Jumali, M. H., Lee, C. H., & Abd-Shukor, R. (2004). Effects of γ-Fe₂O₃ on the transport critical current density of (Bi_{1.6}Pb_{0.4}Sr₂Ca₂Cu₃O₁₀ superconductors. *Journal of Materials Science*, 39(23), 7125-7128.
- Yoshii, K., Fukuda, T., Akahama, H., Kano, J., Kambe, T., & Ikeda, N. (2011). Magnetic and dielectric study of Bi₂CuO₄. *Physica C: Superconductivity and its Applications*, 471(21), 766-769.
- Yu, J., Ishikawa, T., Arai, Y., Yoda, S., Itoh, M., & Saita, Y. (2005). Extrinsic origin of giant permittivity in hexagonal BaTiO₃ single crystals: Contributions of interfacial layer and depletion layer. *Applied Physics Letters*, 87(25), 252904.